Molecular BioSystems

RSC Publishing

PAPER

View Article Online
View Journal | View Issue

Cite this: *Mol. BioSyst.*, 2013, **9**, 3146

Dissecting the salt dependence of the Tus–*Ter* protein–DNA complexes by high-throughput differential scanning fluorimetry of a GFP-tagged Tus†

Morgane J. J. Moreau[ab] and Patrick M. Schaeffer‡*[ab]

Received 15th July 2013,
Accepted 30th September 2013

DOI: 10.1039/c3mb70426b

www.rsc.org/molecularbiosystems

The analysis of the salt dependence of protein–DNA complexes provides useful information about the non-specific electrostatic and sequence-specific parameters driving complex formation and stability. The differential scanning fluorimetry of GFP-tagged protein (DSF-GTP) assay has been geared with an automatic T_m peak recognition system and was applied for the high-throughput (HT) determination of salt-induced effects on the GFP-tagged DNA replication protein Tus in complex with various *Ter* and *Ter-lock* sequences. The system was designed to generate two-dimensional heat map profiles of Tus-GFP protein stability allowing for a comparative study of the effect of eight increasing salt concentrations on ten different *Ter* DNA species at once. The data obtained with the new HT DSF-GTP allowed precise dissection of the non-specific electrostatic and sequence-specific parameters driving Tus–*Ter* and Tus–*Ter-lock* complex formation and stability. The major factor increasing the thermal resistance of Tus–*Ter-lock* complexes in high-salt is the formation of the TT-lock, *e.g.* a 10-fold higher K_{spe} was obtained for Tus-GFP:*Ter-lockB* than for Tus-GFP:*TerB*. It is anticipated that the system can be easily adapted for the study of other protein–DNA complexes.

1. Introduction

The affinity and stability of protein–DNA complexes are characterized by the binding constant and Gibbs energy of binding, but these parameters are not sufficient to dissect the nature of the physical forces involved in the interaction – *i.e.* non-specific electrostatic contacts *vs.* sequence-specific contacts. An experimental approach that analyzed the effects of salt on the stability of protein–DNA complexes was developed nearly four decades ago by Record *et al.*[1,2] It assumes that the release of counter-ions associated with free DNA is a major factor in protein–DNA complex formation.[1–6] The application of the concept of counter-ion condensation (CC) allows determination of the electrostatic component in a protein–DNA complex. The analysis of the salt dependence of the binding constant can also be used to determine the non-electrostatic component of the interaction, which is sequence-specific. The relative magnitude and importance of each component modulates the functional specificity and affinity of a protein for various binding sites.[6] As a rule, the salt resistance of a protein–DNA complex indicates a dominant contribution of sequence-specific interactions.

Tus is a relatively well characterized protein that binds specifically to 21 bp DNA sequences, called *Ter*, scattered around the circular chromosome of *E. coli* (Fig. 1A) to coordinate the termination of DNA replication opposite to *oriC*.[7–22] The Tus–*Ter* complex can only arrest a replisome approaching towards its non-permissive face through the formation of a Tus–*Ter*-lock (TT-lock),[18] whose action is to tighten the complex, avoiding dissociation of Tus. When the replisome approaches the permissive face of the complex, Tus rapidly dissociates from *Ter*. The TT-lock is formed when the C·G(6) base pair is broken during DNA unwinding at the non-permissive face of the complex. The unpaired C(6) can then bind into a cytosine-binding pocket at the surface of Tus.[18] The 'polarity' of the Tus–*Ter* complex has also been proposed to be the result of a specific interaction occurring between Tus and the DnaB helicase at the forefront of the replisome.[7,19] All together, 14 *Ter* sites have been identified.[11] While the role of the innermost strong Tus–*Ter* complexes (Tus–*TerA–D*, Fig. 1A) in DNA replication termination is clear, the presence and organization of the outer *Ter* sites is still enigmatic.[11,16] The characterization of the outer *Ter* sites is therefore of importance to understand their function and role in the wide replication fork trap of *E. coli* (Fig. 1A).

The effect of salt on the association and dissociation kinetics of Tus–*TerB* was previously examined by surface plasmon

[a] *Centre for Biodiscovery and Molecular Development of Therapeutics, James Cook University, Douglas, QLD 4811, Australia*
[b] *Comparative Genomics Centre, James Cook University, Douglas, QLD 4811, Australia*

† Electronic supplementary information (ESI) available. See DOI: 10.1039/c3mb70426b

‡ School of Pharmacy and Molecular Sciences, James Cook University, DB21 James Cook Drive, Townsville, QLD 4811, Australia. E-mail: patrick.schaeffer@jcu.edu.au; Fax: +61 (0)7 4781 6078; Tel: +61 (0)7 4781 4448.

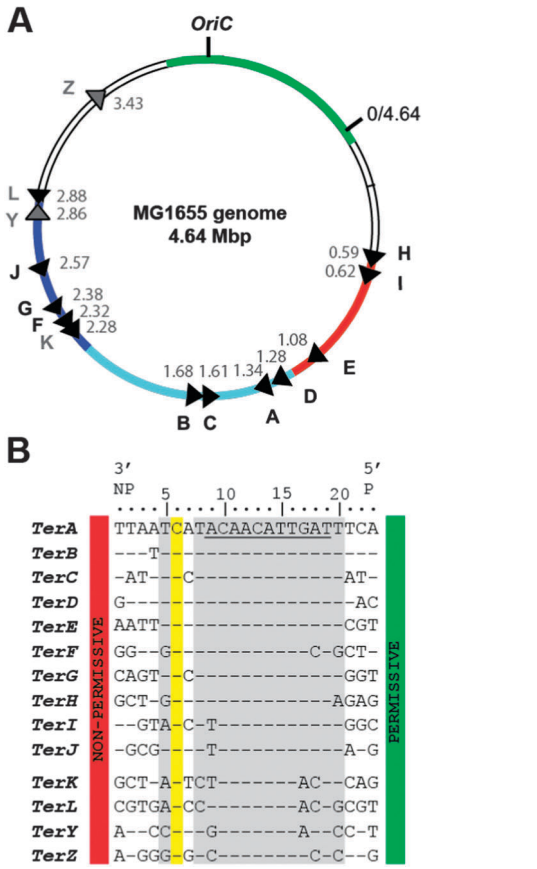

Fig. 1 Position, orientation and sequences of *Ter* sites in *E. coli* MG1655. (A) Map of the *E. coli* genome indicating the approximate positions and orientations of the 14 *Ter* sites.[11] The tip of the arrow indicates the non-permissive face of the Tus–*Ter* complex. The coloured regions on the circle represent chromosome domains: *oriC* (green); unstructured domains (colourless); the right domain (red); the left domain (dark blue); and the termination domain (light blue).[27,28] The numbers inside the circle indicate *Ter* site positions in Mbp. (B) Sequence similarities of the 14 *Ter* sites. The conserved C(6) is highlighted in yellow. Sequences are oriented with their non-permissive face (NP) on the left. Nucleotides interacting with Tus are shaded in grey.[12] The 11-bp core sequence determined by Coskun-Ari and Hill is underlined.[9]

resonance (SPR).[20] Later, the effect of salt on the dissociation kinetics of the TT-lock variant of *TerB* (*Ter-lockB*) was also examined, revealing an increased resistance to salt by this species compared to *TerB*.[18] The kinetic parameters of the primary *Ter* sites, *TerA–J*, and their TT-lock variants have recently been characterized by SPR at two different salt concentrations.[16] Unfortunately, weak binders could not be characterized under high salt conditions and strong binders under low salt conditions. Notably, *TerF* was shown to be only marginally more specific than a non-specific *oriC* DNA fragment, suggesting that *TerF* forms mainly non-specific electrostatic interactions with Tus, and raising questions about its role in DNA replication termination.[16] The study revealed the limitation of using SPR for these studies as the data were complicated by non-specific binding of Tus to the surface of the chip in low salt and extreme bulk shift effect under high salt conditions. Using a newly developed DSF-GTP assay we recently investigated the effect of salt on Tus-GFP:*TerB* and Tus-GFP:*Ter-lockB* complexes.[17] Nevertheless, the limited and scattered data we and others obtained on the effect of ionic strength on the Tus–*Ter* complex prompted us to further investigate this important system.

In this study the effect of very low to high ionic strength on the stability of the ten primary Tus–*Ter* and their Tus–*Ter*-lock complexes was systematically analyzed using DSF-GTP[17] equipped with an automatic T_m peak recognition system. The new automatic T_m peak recognition system is able to automatically generate two-dimensional (2D) heat maps with an accuracy of 96% and greatly accelerates data analysis. Using this system, the effect of increasing concentrations of potassium chloride on the overall stability of these complexes could be determined in high-throughput and revealed the subtle differences in affinity between the different *Ter* species and their TT-lock variants.

2. Materials and methods

2.1. Protein expression and purification

His_6-Tus-GFP was expressed and purified as previously described,[10] however proteins were resuspended in SPR_{250} buffer (50 mM Tris (pH 7.6), 250 mM KCl, 0.1 mM EDTA and 0.2 mM β-mercaptoethanol) and dialysed twice against the same buffer at 4 °C.

2.2. Effect of ionic strength on Tus-GFP:*Ter* complex stability

Tus-GFP was incubated with *Ter* in the presence of various KCl concentrations and subjected to the melting curve program of a real-time thermal cycler (IQ5 iCycler, Bio-rad). For this, equal volumes of Tus-GFP (7.5 μM), hybridized oligonucleotides (9 μM) and KCl (25.5–1050 mM) were mixed in a qPCR 96-well plate (Bio-Rad) to yield final reaction conditions of 50 mM Tris (pH 7.7), 0.1 mM EDTA, 0.2 mM β-mercaptoethanol supplemented with 8.5–350 mM KCl. *Ter* DNA was in slight excess (3 μM) compared to Tus-GFP (2.5 μM). The mixture was left 10 min at room temperature to reach equilibrium before starting the melting curve protocol. The melting curve program was run from 35 °C to 75 °C, 0.5 °C per cycle, 30 s dwell time. The T_m values were obtained from the first peak maximum in the melting curves either by graphical analysis[17] or using the automatic peak recognition program developed with the free RStudio interface (as described below). Experiments were performed in triplicate.

2.3. Automatic T_m peak recognition using RStudio

The following program was adapted from Thermal Shift Assays – Xtalwiki. After a DSF-GTP run, the RFU and −dRFU/d*T* data were exported to Excel and saved as CSV files. The following script commands RStudio to read the CSV files (italicized characters are to be adapted for each user, run or file name).

raw_data<-read.csv("*C:/Documents and settings/path to file/RFUfile*.csv")

grad_data<-read.csv("*C:/Documents and settings/path to file/−dRFUfile*.csv")

The following script commands RStudio to scale plots of RFUs and −dRFU/d*T* on a single graph and determine T_m at the maximum of the derivative function between 35 °C and 71.5 °C to avoid

taking into account the peak corresponding to GFP unfolding. It then generates individual plots for each well in a pdf file.

```
find.tm<-function(temp=temp, I=I, grad=grad, well=well) {
Igrad<-matrix(1:154,nc=2)
Igrad[,1]=I
Igrad[,2]=grad
scaled_data<-scale(Igrad)
plot(x=temp, y=scaled_data[,1], type='p', col='red', xlab="",
ylab="",ylim=c(-5,5))
lines(x=temp, y=scaled_data[,2], type='l', col='blue',
lwd=2,xlab="", ylab="")
title(main=well)
tm.s=temp[which.max(Igrad[1:73,2])]
title(sub=sprintf("Tm=%4.1f", tm.s, cex.sub=1.2))
return(tm.s)}
pdf(file="C:/Documents and settings/username/path to file/
Thermographs.pdf", width=30, height=21, pointsize=9)
layout(matrix(data=1:96, nrow=8, ncol=12, byrow=TRUE))
tma<-matrix(nrow=12, ncol=8)
for(i in 2:97) {try(expr=tma[i-1]<-find.tm(temp=raw_data[,1],
I=raw_data[,i], grad=grad_data[,i], well=names(raw_data)[i]))}
dev.off()
```

It has to be noted that in line 2 of the above script (see the number in bold), the matrix scale has to be adapted for the range of temperatures tested in a particular experiment (*i.e.* ramping speed determines the number of rows in the database) and can be generally calculated as follows: (total number of rows in the dataset − 1) × 2. In the above example, the temperature range was 35 °C to 73.5 °C with 0.5 °C increments. In line 11, the numbers in bold indicate the range of rows corresponding to the temperatures over which the program identifies the highest value on the *y*-axis as T_m. Since the peak corresponding to the unfolding of GFP starts at around 72 °C and rapidly increases, the maximum temperature used for T_m determination was 71.5 °C to avoid false peak identification.

The following script generates a 2D heat map of the 96-well plate with a color gradient code from red (low T_m) to yellow (high T_m):

```
pdf(file="C:/Documents and settings/username/Desktop/
2Dheatmap.pdf", width=6, height=5, paper="a4", pointsize=8)
tmaplot<-matrix(nrow=12,ncol=8,data=0)
for(i in 1:8) {tmaplot[,9-i]=tma[,i]}
image(tmaplot)
dev.off()
```

The correlation between T_m values obtained through the automatic peak recognition system and the visual curve analysis was tested using the Pearson *r* test in GraphPad Prism.

2.4. Determination of the number of ionic contacts and specific interactions K_{spe}

The variation in ionic contacts (N) and K_{spe} was determined for *TerB, Ter-lockB*, *TerF, Ter-lockF*, *TerJ* and *Ter-lockJ.* Tus-GFP (2.5 μM) was incubated with *Ter* or *Ter-lock* DNA at concentrations ranging from 0.6–10 μM in the presence of increasing [KCl] and subjected to the melting curve program of a real-time thermal cycler (IQ5 iCycler, Bio-rad). For this, equal volumes of Tus-GFP (7.5 μM), *Ter* or *Ter-lock* (1.8–30 μM) and [KCl] (450 to 1275 mM) were mixed in a qPCR 96-well plate (Bio-Rad) to yield reactions containing 50 mM Tris (pH 7.5), 0.1 mM EDTA, 0.2 mM β-mercaptoethanol supplemented with 150–425 mM [KCl]. The mixture was left 10 min at room temperature to equilibrate before starting the melting curve protocol. The melting curve program was run from 35 °C to 85 °C, 0.5 °C per cycle, 30 s dwell time. The T_m values were obtained from the first peak maximum in the melting curves using the automatic peak recognition program. Experiments were performed in duplicate.

The DNA-induced stability (ΔT_m) was calculated by subtracting the T_m value obtained for free Tus-GFP from the T_m value obtained for Tus-GFP:*Ter* complexes at a given KCl concentration. $\log K_{obs}$ values were obtained for each [KCl] and *Ter* or *Ter-lock* species as previously described[17] by plotting the ΔT_m *vs.* log[*Ter*] and extrapolation of the linear part of the slope (the intersection of the extrapolated slope with the *x*-axis represents $\log K_{obs}$). The slopes (SK_A) were obtained by linear regression of $\log K_A$ ($K_A = 1/K_{obs}$) *vs.* log[KCl] according to Record *et al.*[2] SK_A values were used to determine the number of cations displaced (N) = $-SK_A/0.88$ and K_{spe} was determined by extrapolation of the SK_A at [KCl] = 1 M.

3. Results and discussion

3.1. Automatic determination of T_m values and generation of 2D heat maps

As a first step, it was essential to increase the throughput of the DSF-GTP assay to be able to handle the volume of data generated in this study. A universal, automatic T_m peak recognition program was developed for the RStudio interface (http://www.rstudio.org) that produces a 2D heat map of a 96-well plate directly from raw data. This script provides individual thermoplots of normalized RFU and −dRFU/dT variables and reports the temperature at the maximum value of the derivative as T_m (see Material and methods and Fig. 2A). The representative thermoplots obtained for free and *TerC*-bound Tus-GFP at increasing [KCl] are shown in Fig. 2A. The T_m values extracted from the thermoplots were then automatically incorporated into 2D-heat maps (Fig. 2B and C).

Due to the prominent GFP peak starting at 72 °C,[17] the melting curves (−dRFU/dT) were analyzed until 71.5 °C to detect the T_m peaks of Tus-GFP complexes – *i.e.* when the GFP signal is minimal in order to reduce the false T_m peak recognition rate. An arbitrary T_m value of 71.5 °C was automatically assigned to peaks at or above this temperature. This was only the case for *Ter*-induced stability of Tus-GFP at the lowest [KCl] (high affinity conditions) with the exception of *TerF* (T_m < 71.5 °C). The T_m values for the remaining *Ter* sites could be visually determined and were generally within 0.5 °C of the arbitrary value. Only for *TerG* and *TerI*, peaks at 73.6 °C and 73.1 °C, respectively, were missed by this method but could be obtained by visual examination. Overall, the data from the automatic peak recognition program correlated well with those obtained by visual determination of T_m for each curve (Fig. 2D). Out of 552 T_m peaks analyzed, only 24 were misidentified by the program, corresponding to an

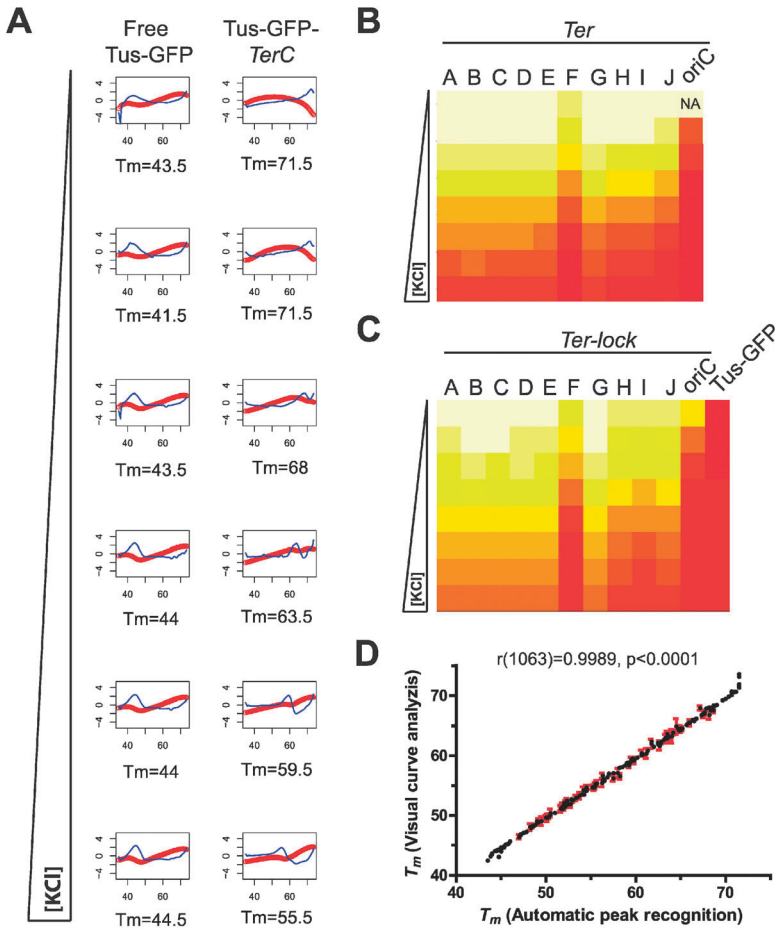

Fig. 2 Automatic determination of T_m for free and DNA-bound Tus-GFP. (A) Examples of thermoplots. RFU signal (red) and its derivative −dRFU/dT (blue) obtained for free or *TerC*-bound Tus-GFP with increasing [KCl] (8.5–250 mM). (B) 2D heat map of T_m values obtained for Tus-GFP:*Ter* complexes with increasing [KCl] (8.5–350 mM). Tus-GFP (2.5 μM) and *Ter* or *oriC* DNA (3 μM) in SPR buffer supplemented with increasing [KCl]. NA: not available. T_m values range: 40 °C (red) to 71.5 °C (pale yellow). (C) 2D heat map for Tus-GFP:*Ter-lock* complexes. (D) Pearson's r correlation between averaged T_m values (n = 3) obtained by visual analysis and by automatic T_m peak analysis of DSF-GTP curves (n = 184; data from free Tus-GFP and in complex with *Ter*, *Ter-lock*, *oriC*, *oriC-lock*). Red error bars: 95% confidence interval.

error rate of 4.3%. Out of these errors, ~50% were due to the GFP peak being higher at 71.5 °C than the Tus-GFP peak, and the remaining errors were from unresolved peaks in the original curves. This error rate could probably be decreased by increasing the protein concentration and accordingly the signal.[17]

The 2D heat map of the 96-well plate provides a colour-coded representation of the experimental screen by transforming T_m values across the plate in a 2-colour gradient code, with the lowest T_m shown in dark red and the highest T_m shown in pale yellow (Fig. 2B and C). The profiles obtained for *TerB* and *Ter-lockB* were in agreement with previous data obtained under the same conditions using a visual analysis method,[16] demonstrating the accuracy of the automatic T_m detection method and its utility for the analysis of high volumes of data.

3.2. Salt resistance of Tus–*Ter* and Tus–*Ter-lock* using a fast 2D DSF-GTP screen

The salt dependence of Tus-GFP in complex with ten *Ter* sites, their *Ter-lock* analogues and a non-specific DNA (*oriC*), was examined in the presence of [KCl] ranging from 8.5–350 mM as previously described for *TerB* and *Ter-lockB*[17] using our improved HT DSF-GTP (Fig. 3). The *Ter-lock* oligonucleotides used in this study are partially single-stranded at their non-permissive side to allow the C(6) to bind into the cytosine-binding pocket of Tus, thus both creating new sequence specific interactions and reducing the overall number of non-specific electrostatic interactions (Fig. 3A, B and 4). When the salt dependence of complex stability of Tus-GFP:*TerB* was previously compared to Tus-GFP:*Ter-lockB* the stability curves crossed, suggesting that the difference in their slopes was the result of TT-lock formation.[17] Here we compared the salt dependence of the remaining *Ter* with their *Ter-lock* species in complex with Tus-GFP to determine if this convenient and fast approach using HT DSF-GTP was able to detect the subtle differences in binding behavior of these species.

As previously observed, the T_m of free Tus-GFP increased moderately and gradually with increasing [KCl] (Fig. 3C–E),[17] indicating that ions bind and stabilize the protein.[5] The non-specific *oriC* and *oriC-lock* increased the stability of Tus-GFP only at low ionic strength (*i.e.* < 150 mM [KCl]) resulting in a ΔT_m > +10 °C at 8.5 mM [KCl] (Fig. 3C and D). The data

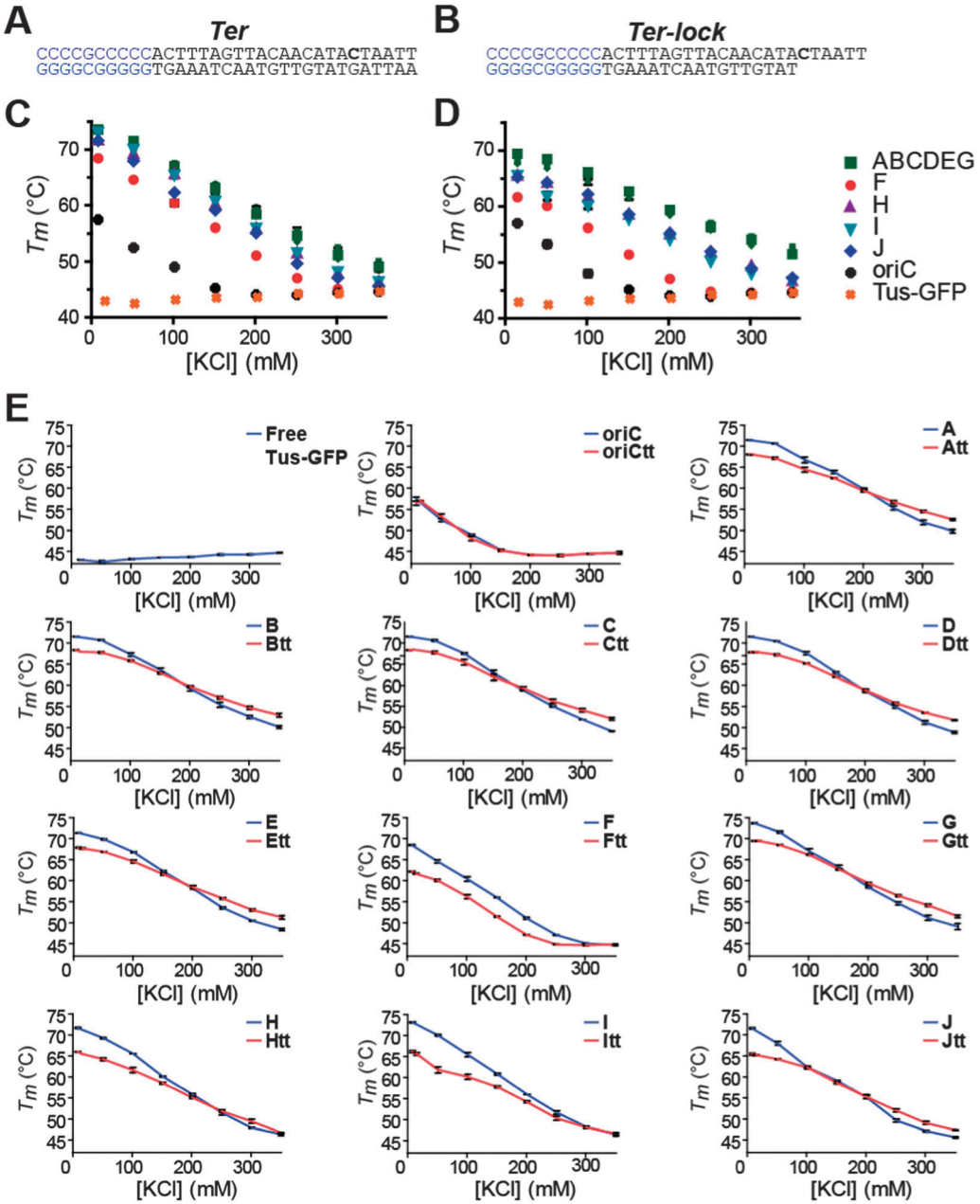

Fig. 3 Effect of ionic strength on Tus-GFP in complex with *Ter* sites or their *Ter-lock* analogues. Representative sequences and structures of *TerA* (A) and *Ter-lockA* (B). Sequences in blue were added to all DNA sequences to increase their melting temperature. Stability curves of T_m *vs.* [KCl] (8.5–350 mM) for Tus-GFP:*Ter* (C) and Tus-GFP:*Ter-lock* (D). The curves obtained for *TerA–E* and *TerG* (C) and their respective *Ter-locks* (D) are almost identical and are represented as a single green square symbol in both panels. *oriC* and *oriC-lock*:Tus-GFP in complex with non-specific DNA. (E) Stability curves were organized in pairs of Tus-GFP:*Ter* (blue) *vs.* Tus-GFP:*Ter-lock* (red; tt) to highlight their differences (n = 3).

highlight that significant intermolecular electrostatic interactions can only occur <150 mM [KCl] between Tus and non-specific DNA. When bound to the strong *TerA–E* and *G*, the T_m of Tus-GFP shifted up to +28 °C at 8.5 mM [KCl]. For these *Ter* sites, the T_m of Tus-GFP decreased gradually with increasing [KCl] due to the gradual breaking of intermolecular electrostatic interactions in the Tus-GFP:*Ter* complexes (Fig. 3C). The salt dependence curves obtained for all strong binders (*TerA–E* and *G*)[16] were similar in shape – *i.e.* similar slopes, amplitudes and maximal T_m (Fig. 3C and Table 1) – suggesting that essentially the same ionic bonds are broken in these complexes. *TerG* binding resulted in the highest T_m at 8.5 mM [KCl], indicating that additional or stronger electrostatic interactions may occur in the Tus–*TerG* complex (Fig. 3E). As expected, the strong *TerA–E* and *G* induced a larger thermal shift than the moderate binders *TerH–J* at almost all salt concentrations, reflecting the higher affinity of Tus for these strong binders (Fig. 3C). Within the weak binders, *TerI* was the only one to be as stabilizing as the strong binders, but only at 8.5 mM [KCl] (Fig. 3C).

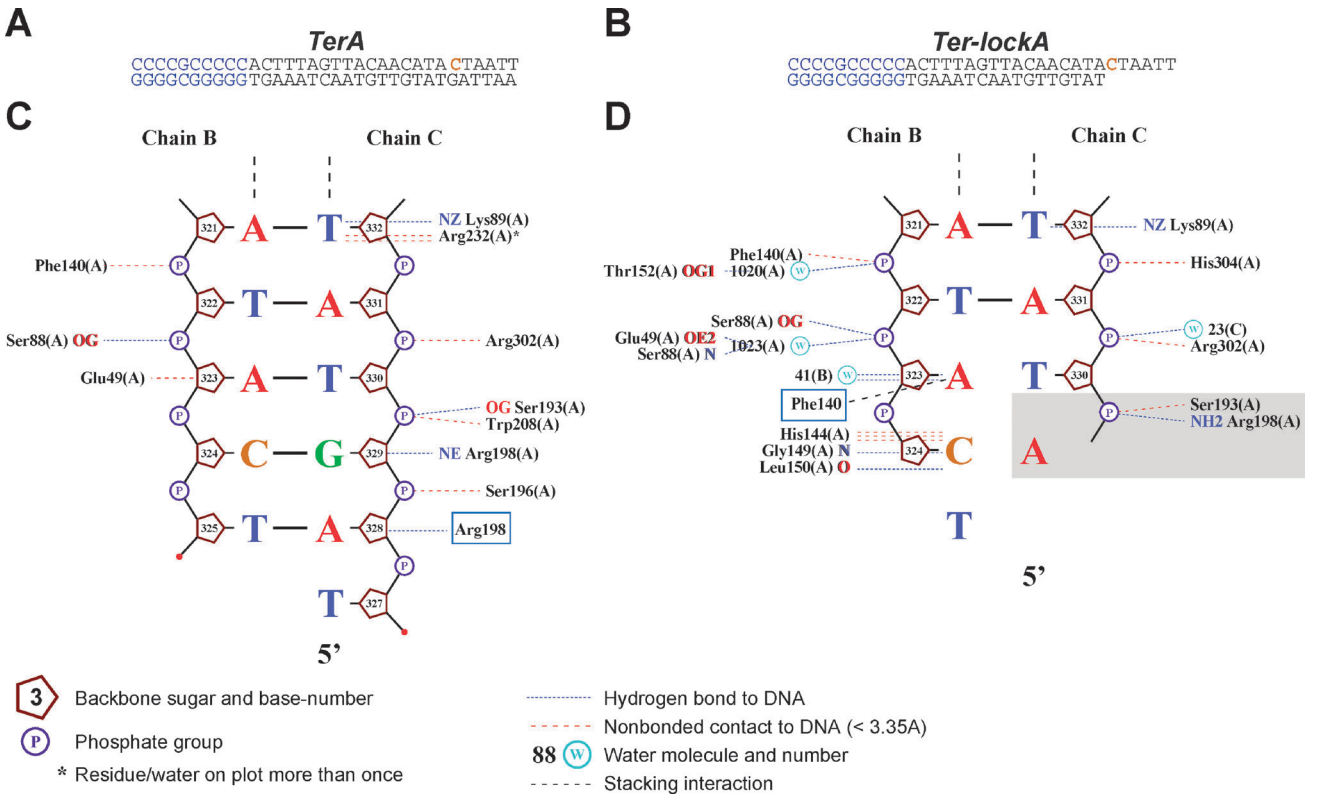

Fig. 4 Protein–DNA interactions at the non-permissive face of Tus. (A) *TerA* sequence. (B) *Ter-lockA* sequence. (C) Details of Tus–*TerA* interactions at the non-permissive face of Tus. (D) Interactions at the non-permissive face of Tus–*Ter-lockA*. Diagrams were adapted from NUCPLOT[29] maps obtained with structural coordinates of PDB2I05 (Tus–*TerA*) and PDB2I06 (Tus–*Ter-lockA*). Boxed residues represent known interactions that were omitted by NUCPLOT. The shaded area (D) highlights the structures and interactions that are absent in our Tus–*Ter-lock* complexes due to the design of *Ter-lock* oligonucleotides used in this study. The C(6) involved in lock formation is represented in orange.

Ter species were systematically more stabilizing than their *Ter-lock* analogues in low salt. This phenomenon has previously been proposed to be due to missing base-specific and electrostatic interactions between G(6)/A(5) and the R198 residue of Tus in the partially single stranded *Ter-locks* compared to the *Ter* species.[16] The R198 residue forms polar and Van der Waals contacts with the deoxyribose moiety of A(5) and G(6) in *Ter* species and a water-mediated ionic interaction with the phosphate group of G(6).[12] It also forms specific hydrogen bonds with these two bases (Fig. 4C) and thus contributes significantly to the overall stability of the complex.[20] The R198A Tus mutant has a 150-fold reduced binding affinity for *TerB* and a lower affinity for non-specific DNA due to its major impact on the association rate constant (k_a), demonstrating the significant contribution of this residue to complex formation rather than complex stability.[20] The higher stability induced by *Ter* compared to *Ter-lock* species in low salt is therefore mainly the result of a decreased association rate constant (k_a) for the Tus–*Ter-lock* complexes. In high salt, ionic contacts are weakened, reducing the difference in k_a between the two species and making the effect of the TT-lock apparent, at least for the strong TT-lock-forming sites.

A shouldering effect was observed in the low-salt part of the curves that was more prominent for the strong *TerA–E* and *G* than the remaining *Ter* sites (Fig. 3E). A steeper negative slope and larger amplitude were observed for *Ter* species than for their *Ter-lock* analogues (Table 1), resulting in the crossing of *Ter* and *Ter-lock* curves between 150–200 mM [KCl] for most TT-lock-forming *Ter* sites (Fig. 3E). This trend immediately suggests a larger contribution of electrostatic interactions in Tus–*Ter* complexes and the presence of additional specific interactions in Tus–*Ter-lock* complexes that increase their salt resistance. Ionic strength affects both specific and non-specific interactions in a protein–DNA complex. However, specific interactions are less severely affected by salt than non-specific interactions.[2,23–26] In high salt, the major factor increasing the resistance of Tus–*Ter-lock* to thermal denaturation is therefore the formation of the TT-lock. Above 150 mM [KCl], when significantly less electrostatic interactions contribute to the stability of the complexes (*i.e.* no binding to non-specific *oriC*), the contribution of the TT-lock is sufficient to overcome and/or surpass the loss of both electrostatic and specific interactions with the nucleotides missing at the non-permissive face of the *Ter-lockA–E and G* species. This is reflected by the crossing of *Ter* and *Ter-lock* curves <200 mM [KCl] for strong TT-lock-forming species.

Ter-lockF was the least stabilizing species after *TerF*. In fact, *TerF* and *Ter-lockF* curves were essentially parallel and did not cross (steepest slopes of -0.94 ± 0.005 and -0.091 ± 0.004 respectively), confirming that *TerF* is the weakest binder and does not form a TT-lock (Table 1 and Fig. 3E).[16] No gain in

Table 1 Effect of ionic strength on Tus-GFP in complex with *Ter* sites and their *Ter-lock* analogues

Ligand	*A*	*B*	*C*	*D*	*E*	*F*[a]	*G*	*H*	*I*	*J*	*oriC*[b]
Ter	−0.085	−0.082	−0.079	−0.081	−0.087	−0.094	−0.085	−0.087	−0.092	−0.095	−0.092
Slope	(0.005)	(0.007)	(0.006)	(0.004)	(0.003)	(0.005)	(0.006)	(0.005)	(0.004)	(0.006)	(0.008)
Max T_m	71.4	71.5	71.6	71.5	71.3	68.4	73.6	71.7	73.1	71.6	57.4
Min T_m	49.8	50.1	49	48.8	48.4	44.6	49	46.3	46.4	45.6	44.6
Amplitude (°C)	21.6	21.4	22.6	22.7	22.9	23.8	24.6	25.4	26.7	26.0	12.8
Ter-lock	−0.057	−0.058	−0.058	−0.061	−0.057	−0.091	−0.063	−0.067	−0.075	−0.066	−0.10
Slope	(0.004)	(0.004)	(0.007)	(0.003)	(0.004)	(0.004)	(0.003)	(0.003)	(0.005)	(0.005)	(0.007)
Max T_m	68.0	68.0	68.5	67.9	67.7	61.6	69.4	65.5	65.6	65.2	57.0
Min T_m	52.5	52.9	52.0	51.7	51.2	44.8	51.5	46.7	46.6	47.3	44.6
Amplitude (°C)	15.5	15.1	16.5	16.2	16.5	16.8	17.9	18.8	19.0	17.9	12.4

Slopes (± SD) were obtained from linear regression of T_m values in the linear portion of the curve. The slopes of all *Ter* and *Ter-lock* curves were taken between 150 and 250 mM [KCl] exept for *TerF*, *oriC* and their respective lock analogues. [a] *TerF* and *Ter-lockF* were analysed between 100 and 200 mM [KCl]. [b] *oriC* and *oriC-lock* were analyzed between 8.5 and 100 mM [KCl]. The max and min T_m values are the T_m at the lowest and highest [KCl], respectively, and the amplitude is the difference between these two values.

thermal stability could be observed for Tus-GFP in complex with *TerF* and *Ter-lockF* at [KCl] > 250 mM and 300 mM respectively. The lower stabilization of Tus-GFP with *Ter-lockF* is probably due to the absence of the interaction between R198 and the G(6) phosphate group (Fig. 4). The low affinity of *TerF* for Tus (previously determined by SPR) raised questions about the biological significance of *TerF*.[16] The comparison of the *TerF* curve with the non-specific *oriC* curve demonstrates that *TerF* has maintained some specificity for Tus (Fig. 3C and D). Indeed, at physiological concentrations (~150 mM [KCl]), *oriC* did not significantly stabilize Tus-GFP, whereas *TerF* induced a thermal shift of +12.5 °C. These data show that *TerF* could still act as a weak pausing site despite its low affinity and its inability to form a TT-lock.

The Tus-GFP stability curves obtained for *TerH–J* and their *Ter-locks* were quite irregular, revealing differences in their electrostatic and specific contributions to Tus-GFP binding. The slopes obtained for *TerI* and *J* were very steep (Table 1) compared to *TerH*. This is probably due to the loss of a specific interaction with T(9), which is mutated to an adenine in *TerI* and *J* (*cf.* Fig. 1B and 4). Within this group, *TerI* binding to Tus-GFP resulted in the highest T_m at 8.5 mM [KCl] suggesting that additional small cooperative electrostatic interactions may occur in the Tus–*TerI* complex (Fig. 3C). Although *TerJ* was most susceptible to ionic strength within this group – suggesting that it forms less specific interactions – *Ter-lockJ* was able to significantly stabilize Tus-GFP and confer a stronger resistance to ionic strength than *Ter-lockI* and *H* (*cf.* Min T_m values in Table 1). Indeed, the stability curves of *Ter-lockJ* and *TerJ* cross at ~200 mM [KCl] whereas the curves obtained for *TerI* and *Ter-lockI*, and for *TerH* and *Ter-lockH*, cross at ~300 and ~250 mM [KCl] respectively (Fig. 3E). *Ter-lockI* produced the steepest slope of all TT-lock-forming *Ter-lock* species. This was surprising given that *TerH* cannot form a significant TT-lock whereas *TerI* can form a moderate TT-lock.[16] While not conclusive, it could be speculated that as *TerI* has a reduced number of specific interactions compared to *TerH* it is more strongly affected by ionic strength.

Overall, the curves obtained with our new approach provided useful comparative information about the relative distribution of specific and electrostatic interactions occurring in the different complexes. Indeed, the comparison of the parameters of the curves such as steepness of the slopes as well as their minimal (min) and maximal (max) T_m in the range of [KCl] tested highlights the differences in ionic and specific interactions occurring in these complexes. The max T_m represents the total contribution of both ionic and specific interactions in the complex at low salt. The ionic interactions are gradually broken when [KCl] increases, indicating that complexes with a comparatively higher min T_m at high [KCl] indicate that they form more specific interactions than species with lower min T_m. Here, the differences in slopes and crossing points of the curves obtained for a given Tus-GFP:*Ter* and its Tus-GFP:*Ter-lock* complex correlate well with an increase in specific interactions resulting from TT-lock formation (Fig. 3). This approach could be very valuable for mutational studies to rapidly identify the ionic and specific interactions occurring in protein–DNA complexes.

3.3. Dissecting the ionic and specific contributions in Tus–*Ter* and Tus–*Ter-lock*

The number of ionic contacts N and the sequence-specific affinity parameter K_{spe} were determined for Tus-GFP with a subset of representative *Ter* sites and their respective *Ter-lock* variants; *i.e.* the strong *TerB*, the weak *TerF*, and the moderate *TerJ*. For this, K_{obs} values were determined at various [KCl] as previously described (Table S1, ESI†)[17] to determine the slopes SK_A = dlog(1/K_{obs})/dlog[KCl]. Within the range of [KCl] tested, the K_{obs} obtained with DSF-GTP reflected the K_D previously obtained by SPR for these species.[16] To calculate N, SK_A values were divided by 0.88, a factor previously used for the Tus–*TerB* complex in the same buffer.[20] The SPR study by Neylon *et al.* revealed that 13 cations were displaced upon binding of Tus to *TerB*. Here, using our DSF-GTP we obtained N = 11 (Fig. 5). This number correlates better with the fact that there are only eight direct ionic contacts[12,20] between lysine or arginine residues and DNA phosphate groups observed in the crystal structure, and that the maximum number of direct and indirect ionic contacts that could potentially form in Tus–*TerB* complex is 14.[20] The N-values that we obtained for the 6 species ranged between 10 and 13 (Fig. 5B). As expected, the SK_A values obtained for

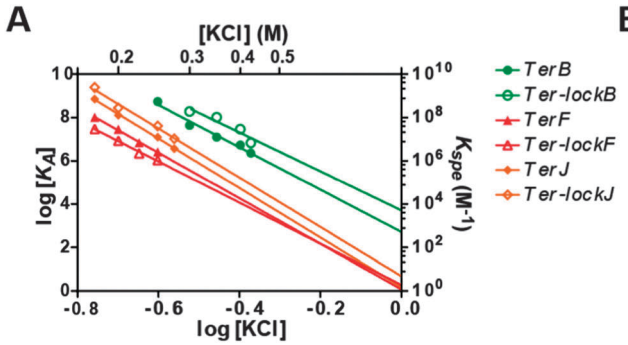

B

Ter	Slope (±SD)	N	Log(K_{spe}) (±SD)	K_{spe}
TerB	-9.8 (±0.9)	11	2.7 (±0.4)	526
Ter-lockB	-9.0 (±2.2)	10	3.7 (±1.0)	5200
TerF	-10.5 (±0.4)	12	0.08 (±0.3)	1.2
Ter-lockF	-9.5 (±0.5)	11	0.3 (±0.4)	1.9
TerJ	-11.4 (±0.4)	13	0.2 (±0.2)	1.5
Ter-lockJ	-11.4 (±1)	13	0.7 (±0.7)	4.8

Fig. 5 Ionic and specific contributions in Tus-GFP:*Ter* and Tus-GFP:*Ter-lock*. (A) Log–log plot of Tus-GFP:*Ter* and Tus-GFP:*Ter-lock* DNA binding constants ($K_A = 1/K_{obs}$) as a function of [KCl]. (B) Determination of *N* and K_{spe} values for Tus-GFP in complex with *TerB*, *F* and *J* and their *Ter-lock* variants. SD: standard deviations ($n = 2$).

Tus-GFP:*TerB* and Tus-GFP:*TerF* were systematically steeper than for their respective Tus-GFP:*Ter-lock* variant suggesting that only one ionic contact was missing in these complexes. This is most likely due to the missing electrostatic interaction involving R198 in the partially single stranded *Ter-lock* species (Fig. 4). Interestingly, Tus-GFP:*TerJ* and Tus-GFP:*Ter-lockJ* have the same *N* value of 13 suggesting that more ionic contacts are formed in these complexes than in Tus-GFP:*TerF* ($N = 12$) and Tus-GFP:*TerB* ($N = 11$). It also suggests that the missing electrostatic interaction involving R198 is not occurring in Tus–*TerJ* and that additional ionic interactions can occur in these complexes. It can therefore be argued that the polar base-specific contacts that are broken upon binding of Tus to the moderate and weak *Ter* binders could rearrange to form new direct or water-mediated electrostatic interactions.

The relative values of K_A (*i.e.* $1/K_{obs}$) at any given [KCl] indicate the contribution of the specific component K_{spe} and the ionic component to the free energy of binding. As a result, when [KCl] = 1 M, the extrapolated $K_A = K_{spe}$. The K_{spe} values obtained for Tus-GFP in complex with the three tested *Ter* and *Ter-lock* pairs are in the following order: K_{spe} for *Ter-lockB* ≫ *TerB* ≫ *Ter-lockJ* > *Ter-lockF*, *TerJ*, *TerF* (Fig. 5) in reasonable agreement with previous data.[16] The K_{spe} obtained with *Ter-lockF*, *TerJ* and *TerF* were very low, highlighting that when in complex with Tus these species form interactions that are mostly ionic. Although, caution must be taken when interpreting these data as the standard deviations are very high in these experiments. Most significant was the 10-fold higher K_{spe} for Tus-GFP:*Ter-lockB* than for Tus-GFP:*TerB* highlighting the specific contribution of TT-lock formation to overall complex stability.[18] As expected, no significant difference in K_{spe} was observed between Tus-GFP:*Ter-lockF* and Tus-GFP:*TerF*, confirming that *Ter-lockF* cannot induce formation of a TT-lock.[16] Finally, a 3-fold higher K_{spe} was observed for Tus-GFP:*Ter-lockJ* than for Tus-GFP:*TerJ*, indicating that the moderate *Ter* sites are not able to form a strong TT-lock.

4. Conclusion

This is the first comprehensive study examining the effect of ionic strength on the primary Tus–*Ter* and Tus–*Ter-lock* complexes using our HT DSF-GTP assay. The data revealed that the major factor increasing the resistance of Tus–*Ter-lock* complexes to thermal denaturation in high-salt is the formation of the TT-lock.[18] This was supported by a 10-fold higher K_{spe} for Tus-GFP:*Ter-lockB* than for Tus-GFP:*TerB*. The data were readily analyzed using a new automatic T_m peak recognition protocol that we adapted to the DSF-GTP assay. The system is very accurate (96% of T_m peaks recognized) with most of the imprecision occurring >71.5 °C. Using this 2D screen format, *i.e.* salt *vs.* ligand, we were able to measure and analyze the effect of 8 [KCl] on 11 different Tus-GFP:DNA complexes and free Tus-GFP simultaneously in a 96 well format and in less than 2 hours. It is important to note that these data could not have been obtained by SPR due to instrumental and surface limitations. Taken together, these results illustrate that electrostatic interactions play an important role in the Tus–*Ter* complex formation and its stability. The system was able to detect subtle differences in overall Tus–*Ter* stabilization that could be attributed to the differences in specific and non-specific interactions occurring between Tus and the various *Ter* sites and their respective TT-lock forming capacity. The weakest *TerF* is the most susceptible to ionic strength followed by *TerJ*, *TerI* and *TerH*. *TerA–C* are the most specific sites based on their stabilizing effects at all salt concentrations, and *Ter-lockB* is the most salt-resistant site. Finally, we are confident that our fast 2D DSF-GTP screen approach will provide an invaluable comparative tool to study and decipher the mode of binding of other DNA-binding proteins and to examine the effect of mutations on complex stability at both DNA and protein levels.

Acknowledgements

P.M.S. acknowledges support from the Smart Futures Fund of the Queensland Government, NIRAP. M.J.J.M. was supported by a JCU postgraduate research scholarship.

References

1 M. T. Record Jr., C. F. Anderson and T. M. Lohman, *Q. Rev. Biophys.*, 1978, **11**, 103–178.
2 M. T. Record Jr., J. H. Ha and M. A. Fisher, *Methods Enzymol.*, 1991, **208**, 291–343.

3 G. S. Manning, *Q. Rev. Biophys.*, 1978, **11**, 179–246.
4 M. T. Record Jr., M. L. Lohman and P. De Haseth, *J. Mol. Biol.*, 1976, **107**, 145–158.
5 T. T. Waldron, G. L. Schrift and K. P. Murphy, *J. Mol. Biol.*, 2005, **346**, 895–905.
6 P. L. Privalov, A. I. Dragan and C. Crane-Robinson, *Nucleic Acids Res.*, 2011, **39**, 2483–2491.
7 D. Bastia and S. K. Singh, *Bioarchitect*, 2011, **1**, 24–28.
8 D. Bastia, S. Zzaman, G. Krings, M. Saxena, X. Peng and M. M. Greenberg, *Proc. Natl. Acad. Sci. U. S. A.*, 2008, **105**, 12831–12836.
9 F. F. Coskun-Ari and T. M. Hill, *J. Biol. Chem.*, 1997, **272**, 26448–26456.
10 D. B. Dahdah, I. Morin, M. J. Moreau, N. E. Dixon and P. M. Schaeffer, *Chem. Commun.*, 2009, 3050–3052.
11 I. G. Duggin and S. D. Bell, *J. Mol. Biol.*, 2009, **387**, 532–539.
12 K. Kamada, T. Horiuchi, K. Ohsumi, N. Shimamoto and K. Morikawa, *Nature*, 1996, **383**, 598–603.
13 D. L. Kaplan, *Curr. Biol.*, 2006, **16**, R684–R686.
14 M. J. Moreau, I. Morin and P. M. Schaeffer, *Mol. BioSyst.*, 2010, **6**, 1285–1292.
15 M. J. Moreau and P. M. Schaeffer, *Analyst*, 2012, **137**, 4111–4113.
16 M. J. Moreau and P. M. Schaeffer, *Mol. BioSyst.*, 2012, **8**, 2783–2791.
17 M. J. J. Moreau, I. Morin, S. P. Askin, A. Cooper, N. J. Moreland, S. G. Vasudevan and P. M. Schaeffer, *RSC Adv.*, 2012, **2**, 11892–11900.
18 M. D. Mulcair, P. M. Schaeffer, A. J. Oakley, H. F. Cross, C. Neylon, T. M. Hill and N. E. Dixon, *Cell*, 2006, **125**, 1309–1319.
19 S. Mulugu, A. Potnis, Shamsuzzaman, J. Taylor, K. Alexander and D. Bastia, *Proc. Natl. Acad. Sci. U. S. A.*, 2001, **98**, 9569–9574.
20 C. Neylon, S. E. Brown, A. V. Kralicek, C. S. Miles, C. A. Love and N. E. Dixon, *Biochemistry*, 2000, **39**, 11989–11999.
21 C. Neylon, A. V. Kralicek, T. M. Hill and N. E. Dixon, *Microbiol. Mol. Biol. Rev.*, 2005, **69**, 501–526.
22 P. M. Schaeffer, M. J. Headlam and N. E. Dixon, *IUBMB Life*, 2005, **57**, 5–12.
23 L. E. Engler, K. K. Welch and L. Jen-Jacobson, *J. Mol. Biol.*, 1997, **269**, 82–101.
24 M. M. Garner and D. C. Rau, *EMBO J.*, 1995, **14**, 1257–1263.
25 R. M. Saecker, in *eLS*, John Wiley & Sons, Ltd., 2001.
26 N. Y. Sidorova and D. C. Rau, *Proc. Natl. Acad. Sci. U. S. A.*, 1996, **93**, 12272–12277.
27 H. Seitz, C. Weigel and W. Messer, *Mol. Microbiol.*, 2000, **37**, 1270–1279.
28 M. Valens, S. Penaud, M. Rossignol, F. Cornet and F. Boccard, *EMBO J.*, 2004, **23**, 4330–4341.
29 N. M. Luscombe, R. A. Laskowski and J. M. Thornton, *Nucleic Acids Res.*, 1997, **25**, 4940–4945.

